Magnetoelectric Sensors

Subjects: Materials Science, Ceramics

Contributor: Zhaoqiang Chu

Multiferroic magnetoelectric (ME) materials with the capability of coupling magnetization and electric polarization have been providing diverse routes towards functional devices and thus attracting ever-increasing attention. The typical device applications include sensors, energy harvesters, magnetoelectric random access memories, tunable microwave devices and ME antennas etc. Among those application scenarios, ME sensors are specifically focused in this review article. We begin with an introduction of materials development and then recent advances in ME sensors are overviewed. Engineering applications of ME sensors are followed and typical scenarios are presented. Finally, several remaining challenges and future directions from the perspective of sensor designs and real applications are included.

Keywords: multiferroic ; magnetoelectric ; sensors ; object detection ; magnetic localization ; current sensing ; biological magnetic measurement ; non-destructive testing ; displacement sensing

1. Introduction

Multiferroic materials have been recently attracting ever-increasing attention because of the capability of coupling at least two ferric orders, i.e., ferroelectricity, ferromagnetism, or ferroelasticity, and the vast potential for multifunctional devices applications [1][2][3][4][5]. A control of polarization P by external magnetic field H (direct ME (DME) effect) or a manipulation of magnetization M by an electric field E (converse ME (CME) effect) can be realized in multiferroic magnetoelectric (ME) materials [6]. Compared with single-phase ME material, ME heterostructures and ME laminates perform greatly enhanced coupling capability, which is generally characterized by ME coefficient *αME* [7][8][9]. After a development of nearly half a century, tremendous progress regarding ME composites and related device applications has been reported [1][2][3][6][10][11][12][13][14][15][16][17][18][19].

2. Materials for ME Sensors

The ME effect was first experimentally demonstrated in single-phase multiferroic material Cr_2O_3 in 1961 [20][21]. After that, diverse studies all over the globe were conducted to further enhance the coupling capability of ferroelectric and magnetic orderings in a single-phase material system [20][22], but the low Curie temperature and the weak ME coupling capability in single-phase ME materials, such as $BiFeO_3$, $BiMnO_3$ and $LuFe_2O_4$, greatly limited their applications [1][23][24]. The proposal of a product effect in composite ME materials by combining the piezomagnetic and piezoelectric effects of ferromagnetic and ferroelectric materials then provided new routes towards improved ME coupling performance. Early in 1986, Pantinakis et al. proposed 2-2 type ME composites based on the aforementioned product effect [25] and giant ME coefficients were gradually realized in laminated ME composites starting from the beginning of 21st century [1][6][10]. Compared with single-phase or 0-3 typed ME materials, 2-2 typed ME composites, such as a bulk ME laminates with piezoelectric phase ($Pb(Zr,Ti)O_3$(PZT), $Pb(Mg,Nb)O_3$-$PbTiO_3$ (PMN-PT)) embedded in piezomagnetic materials (FeCoSiB, FeBSiC Terfenol-D, Ni or Fe-Ga) [8] and a FeGaB/AlN thin-film ME heterostructure [26], exhibited enhanced ME coupling performance benefitting from the removal of the leakage current and the improvement of the interfacial strain transfer. At this section, we will first review materials advances in ME sensors since 2002.

2.1. Bulk ME Laminates

It is highly desirable to design new connectivity structures for circumventing the limitation of leakage current that occurs in 0-3 typed ME composites. Back in 2002, Ryu et al. developed a laminated Terfenol-D/PZT/Terfenol-D ME composite (Figure 1a) with 2-2 type connectivity to solve the leakage current problem in 0-3 type ME composites, and the obtained ME coupling coefficient at non-resonance frequency reached as high as 5 V/cm·Oe [27]. This was a significant event in the development of ME laminates and various kinds of laminated structures were proposed afterwards [10][27]. For example. Dong et al. reported 2-2 type ME laminates consisting of Terfenol-D ferrite and PMN-PT piezoelectric crystal. These ME composites work with L-T mode and display relatively low ME coefficients of 2.2 V/cm·Oe at non-resonance frequency [28]. In a bid to further improve the ME voltage coefficient, Dong et al. in 2005 first proposed a push-pull mode that increased

the distance between electrodes and decreased the static capacitance of ME laminates from nF to pF scale [29][30]. In such 2-2 type ME composites, the piezoelectric core was symmetrically poled along its longitudinal direction and rgw d_{33} piezoelectric constant of a piezoelectric material could be utilized. A giant ME voltage coefficient of 1.6 V/Oe at non-resonant frequencies was observed experimentally [30]. One year later, Dong et al. further developed a multi-push-pull mode in 2-1 ME composites. The schematic structure configuration and operation mode of such a 2-1 ME composite is presented in Figure 1c. It consisted of a piezo-fiber layer laminated between FeBSiC alloys. For the first time, the non-resonant ME coefficient at 1 Hz reached 22 V/cm·Oe, making such a structure especially suitable for low-frequency and passive magnetic sensing [31][32][33][34][35], but it should be noted here that the mechanical quality factor for such a 2-1 type ME composites is normally less than 100, so ultra-high resonant ME coefficients cannot be realized in this case [29].

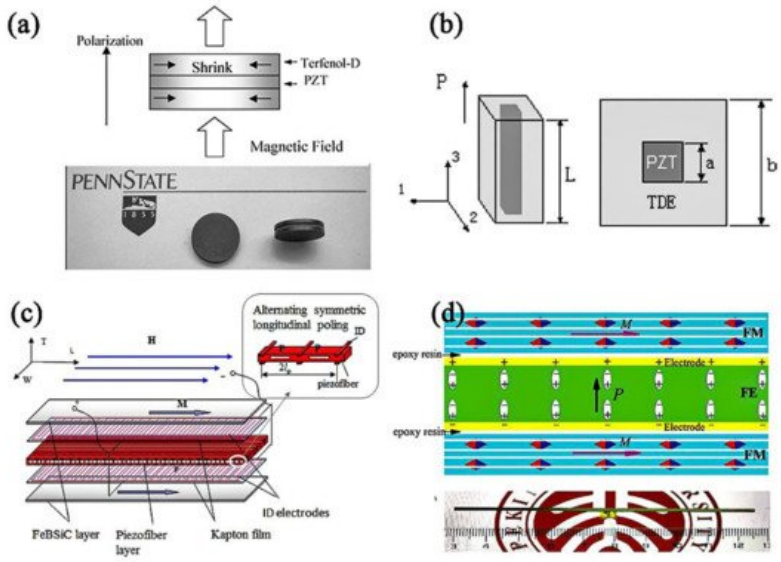

Figure 1. (**a**) Schematic structure (top) and photograph (bottom) of ME laminate composites using Terfenol-D and PZT disks [27]. (**b**) 3D and crosss ectional schematic illustration of the single period of 1-3-type ME structure [36]. (**c**) Illustration of the FeBSiC/piezofiber laminate configuration working on multi-push-pull mode [29][30]. (**d**) The schematic view for 1-1 laminated ME composite and a-(ii) the prototype snapshot of the 1-1 typed ME sample [8].

Another way to address the difficulty of fully polarizing the piezoelectric phase in 0-3 type ME composites is replacing the particle phase with a 1-D piezoelectric fiber (forming 1-3 typed connectivity). For example, in 2005 Nan et al. reported a 1-3 type ME composite with ZT rod arrays embedded in a Terfenol-D medium via a dice-and-fill technique. The non-resonant ME coupling coefficient reached 6.2 V/cm·Oe [37], which represented great progress for ME composites. Two years later, Ma et al. simplified this 1-3 type ME structure by just embedding one single PZT rod in a Terfenol-D/epoxy mixture [36]. The single period element of the 1-3 ME composites is shown in Figure 1b. Although the non-resonant ME coupling coefficient decreased by almost one order of amplitude, this simple structure, low-cost fabrication process and sub-millimeter size made it attractive for micro-ME array applications [36].

In 2017, Chu et al. reported a 1-1 type ME composites, which consisted of a [011]-oriented $Pb(Mg,Nb)O_3$-$PbZrO_3$-$PbTiO_3$ (PMN-PZT) single crystal fiber and laser-treated amorphous alloy Metglas. The 1-1 type ME composite featured the one-dimensional configuration as shown in Figure 1d [8]. The laser treatment could decrease magnetic hysteresis loss of Metglas and thereby enhance the Q value of the ME resonator. In addition, the fiber configuration effectively utilized the magnetic flux concentration effect occurring in Metglas layers. More importantly, this 1-D configuration favored the longitudinal vibration mode of ME laminates. A ME coupling coefficient of ~7000 V/cm·Oe, that was nearly seven times higher than the best result published previously, was finally realized, opening a door to develop new ME devices, e.g., resonant magnetic receivers in particular [8]. In addition, a high ME coefficient of 29.3 V/cm·Oe at non-resonant frequency was also achieved for our 1-1 type composites. Note, only one single crystal was consumed in this case, while previous 2-1 type composites normally took five crystals. In 2020, the resonant ME coefficient of 1-1 type ME composites was further enhanced to 12,500 V/cm·Oe by using a hard piezo-crystal Mn-PMN-PZT [9]. A summary of the field coupling coefficient of different ME laminates, i.e., 0-3, 2-2, 2-2.1-1 ME laminates, is given in Table 1.

Table 1. Some ME laminates and their ME coupling performances.

Composition	Year	Connectivity	Working Mode	$\alpha_{ME}^{non-resonance}$ $(\mathbf{V/cm \cdot Oe})$	$\alpha_{ME}^{resonance}$ $(\mathbf{V/cm \cdot Oe})$
Terfenol-D/PZT [36]	2007	3-1	L-L	0.5	18.2
$NiFe_2O_4$/PZT [38]	2001	2-2	L-T	1.5	/
Terfenol-D/PZT [27]	2002	2-2	L-T	5	/
Metglas/PVDF [39]	2006	2-2	L-T	7.2	310
Metglas/P(VDF-TrFE) [40]	2011	2-2	L-L	17.7	383
Lanthanum gallium tantalite/ permendur [41]	2012	2-2	/	2.3	720
FeCoSiB/(Pt)/AlN in vacuum [42]	2013	2-2	L-T	/	20,000
FeCoSiB/(Pt)/AlN [43]	2016	2-2	L-T	/	5000
Metglas/LiNbO3 [44]	2018	2-2	L-T	1.9	1704
FeBSiC/PZT [30]	2006	2-1	L-L	22	500
Metglas/PMN-PT [31]	2011	2-1	L-L	45	1100
Metglas/PMN-PT without laser treatment [8]	2017	1-1	L-T	29.3	5500
Metglas/PMN-PT with laser treatment [8]	2017	1-1	L-T	22.9	7000
Metglas/Mn-PMN-PZT with laser treatment [9]	2020	1-1	L-T	23.6	12,500

Note: *Connectivity.* We use different number to represent the connectivity of each individual phase. For example, 1-3 type composite means one-phase fiber (denoted by 1) was embedded in the matrix of another phase (denoted by 3); 2-2 type composite means laminated structure (each phase has a plane configuration denoted by 2); 2-1 type composite means one-phase fiber was laminated with another phase plate; 1-1 type means both phases are in the form of fiber configuration. *Working mode.* L-L, L-T means longitudinal vibrations with longitudinal magnetization and transverse polarization(L-L) or transverse magnetization and transverse polarization (L-T).

With respect to ceramic-based thin film multiferroic laminates, Ryu et al. recently developed a $Pb(Zr,Ti)O_3$ film deposited on piezomagnetic materials, e.g., Ni and Metglas. The crystallization of PZT film was implemented by laser annealing,

which was able to keep the piezomagnetic layer free from property degradation [45][46][47][48]. Readers can get access to more detailed information concerning film-based ME composites in other review papers [3][6][10].

2.2. MEMS and NEMS ME Laminates

In a bid to obtain miniaturized ME devices with enhanced ME coupling capability, micro-electro-mechanical systems (MEMS) fabrication technology is a promising approach benefiting from the strong interfacial bonding force and the fine control over the material composition. Greve et al. developed a thin film MEMS composite consisting of AlN and amorphous $Fe_{90}Co_{78}Si_{12}B_{10}$ [49]. AlN is an ideal piezoelectric material compatible with MEMS techniques, and amorphous soft magnetic alloy is a good candidate for the piezomagnetic phase because of its high piezomagnetic properties. As shown in Figure 2a,b, two kinds of deposition flow could be used for MEMS ME composites. Conventional process flow involves the deposition of a high temperature constituent (AlN). In Figure 2a, a reverse flow was then proposed, where FeCoSiB was deposited as the first layer on the smooth wafer surface and AlN, including with the Pt seed layer, was deposited on top of it without any substrate heating [43]. A giant ME coupling coefficient of 5000 V/cm·Oe was measured in this case [43]. In Figure 2b, depositing the magnetostrictive layer and the piezoelectric layer on two sides of a silicon substrate separately is another way to obtain good MEMS ME films [50]. With respect to NEMS ME films, Sun's group in Northeastern University has contributed lots of works in this field [26][51][52]. As shown in Figure 2c,d, the typical material is AlN and FeGaB film. As a ME resonator, both laterally-vibrating (Figure 2c) or vertically-vibrating (Figure 2d) mode can be realized at different frequency bands. Recently, a NEMS ME resonator has been successfully utilized for mechanical antennas with miniaturized size compared with traditional antennas driven by RF current [53].

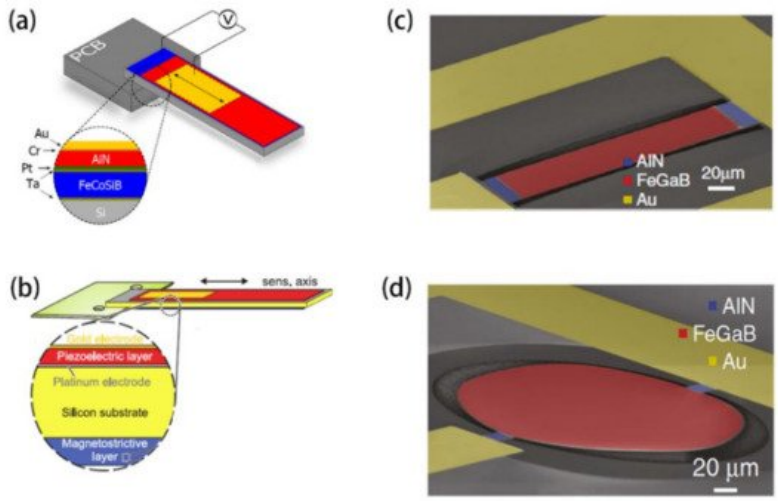

Figure 2. Sketch of ME MEMS cantilever with the functional layer deposited on one side (**a**) [43] and two side (**b**) [50] of silicon substrate. (**c**) Scanning electron microscopy (SEM) images of the ME nano plate resonator. (**d**) Scanning electron microscopy (SEM) images of the fabricated ME thin-film bulk acoustic wave resonators. The red and blue areas show the suspended circular plate and AlN anchors. The yellow area presents the electrode [53].

3. Advances in ME Sensors

The giant ME coupling in ME composites provides the chances to be implemented as diverse functional devices, such as sensors, energy harvesters, magnetoelectric random access memories, tunable microwave devices and ME antennas, etc. Among those application scenarios, advances in ME sensors will be reviewed here.

To assess the performance of a general magnetic sensor, several critical parameters should be considered, i.e., limit of detection (LoD), sensitivity, working temperature, dynamic range, power consumption, size and the cost, but one should note LoD and sensitivity should be given a high priority when taking the research stage of ME sensors into consideration. With respect to the LoD of ME sensors, the ME coupling coefficient and the voltage noise level should be considered equally. Table 1 summarizes the ME coefficients of typical ME composites. The total noise level *Nt* comes from both internal and external noise sources. The internal noise is dominated by the dielectric loss *NDE* and the leakage resistance *NR*, which can be written as follows [32][33]:

$$N_t = \sqrt{N_{DE}^2 + N_R^2} = \sqrt{\frac{4kTC_p \tan\delta}{2\pi f} + \frac{1}{(2\pi f)^2}\frac{4kT}{R}}, \quad (1)$$

where k is the Boltzmann constant (1.38×10^{-23} J K^{-1}), T is the temperature in Kelvin, C_p is the static capacitance, tan δ is the dielectric loss, f is the frequency in Hz and R is the DC resistance of the ME sensor. The total noise density *Nt* has a 1/f spectrum and makes the magnetic field detection at low frequency much more difficult. On the other hand, ME sensors are susceptible to external environment variations, e.g., temperature fluctuation and base vibration, which typically occurs in low frequency as well [7][54]. We will discuss the current advances in ME sensors focusing on the improvement of LoD in the following sections.

3.1. Low-Frequency Magnetic Sensor

In 2011, Wang et al. reported the realization of an extremely low limit of detection through a combination of giant ME coupling in 2-1 type ME composites and a reduction in each noise source. Giant ME coupling was achieved by optimizing the stress transfer in multi-push-pull mode, the thickness ratio of Metglas to piezofiber, and the ID electrodes distribution on Kapton (Figure 3a). Experimental results showed that an extremely low equivalent magnetic noise of 5.1 pT/√Hz at 1 Hz was obtained (Figure 3b) [33].

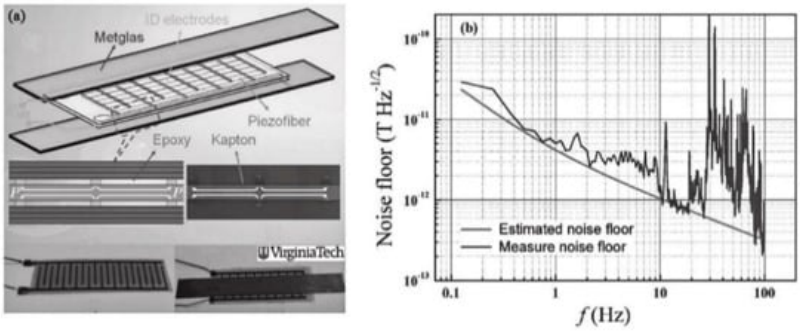

Figure 3. (**a**) Schematic diagram and the protype photo of 2-1 type ME composite working on multi-push-pull mode. (**b**) Measured and estimated equivalent magnetic noise of the proposed sensor unit [33].

The problem in 2-1 type ME composites based on multi-push-pull working mode is the difficulty to fully polarize the piezoelectric phase and the capacitance in this configuration is usually small. In 2012, Li et al. further pointed out that the equivalent magnetic noise could be reduced by a factor of √N through stacking some number N of ME sensor units in parallel [32]. From the perspective of reducing the total noise level *Nt*, connecting N ME sensor units in series could be also effective to increase the detection capability. For example, Fang et al. reported a 2-1 ME sensor based on multi-L-T mode, of which the schematic is shown in Figure 4a,b [55]. In this case, the ME charge coefficient could be kept at a high level while the static capacitance and the leakage current could be decreased remarkably by increasing the number (N) of piezoelectric crystal. As a result, the measured equivalent magnetic noise (EMN) of the Metglas/Mn-PMNT composite was as low as 0.87 pT/√Hz at 30 Hz for N = 7, which was 1.8 times lower than that for N = 1 (see Figure 4c,d) [55].

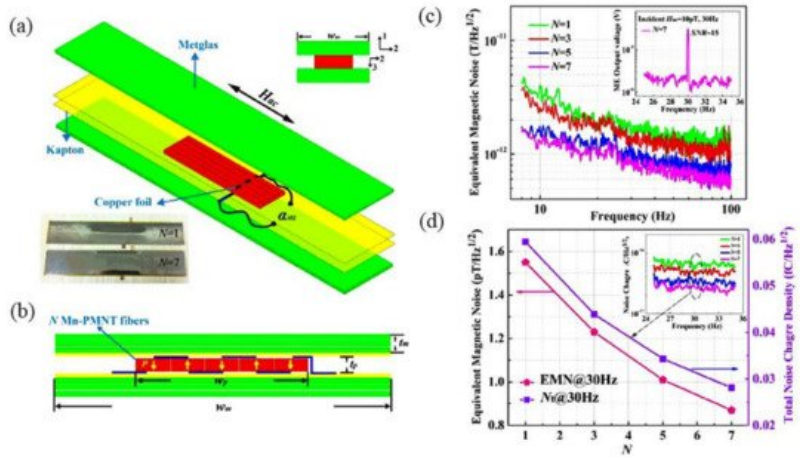

Figure 4. 3D structure of Metglas/Mn-PMNT ME composite (**a**) and its cross-sectional diagram (**b**); (**c**) The EMN over the frequency range of 8 Hz < f < 100 Hz. (**d**)The EMN and *Nt* of different Metglas/Mn-PMNT sensors at 30 Hz [55].

In 2011, frequency conversion technology (FCT) was proposed to circumvent the large 1/f noise for active ME sensors [56][57][58][59][60]. Quasi-static or extremely-low frequency magnetic fields can be effectively detected in this case. For example, Chu et al. realized a limit of detection of 33 pT/√Hz at 0.1 Hz by using amplitude modulation method combined with FCT in 1-1 type magnetoelectric composites [61]. During the measurement, a carrier signal and a modulation signal were both applied to the ME sensor.

Figure 5a,b demonstrates the fundamental modulation phenomenon and the block diagram of the correlation detection scheme with respect to an amplitude modulation signal S_{Mod} (t). The output voltage waveform was observed by a mixed signal oscilloscope. The ME sensor was driven by 100 Hz carrier signal and the modulation frequency is 10 Hz. Once the low-frequency modulation field H_{AC} with an intensity of 10^{-6} T was applied, a clear amplitude modulation (envelope) signal was generated due to the intrinsic frequency mixing characteristic in ME sensors, as shown in Figure 5a(ii).

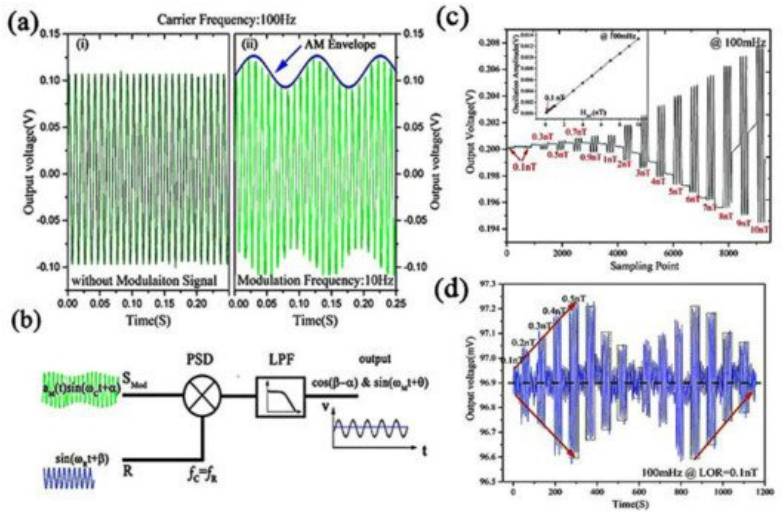

Figure 5. (**a**) The demonstration of fundamental modulation and frequency mixing phenomenon in ME sensors; (**b**) A block diagram of the amplitude demodulation method with respect to amplitude modulation signal S_{Mod} (t). (**c**) The measured output waveform in response to an applied weak AC magnetic field at 100 mHz. (**d**) A linear-response to varying H_{AC} at 100 mHz with a step of 0.1 nT [55].

In order to test the limit of detection by using this amplitude modulation method, the time constant decreased to 10 ms and the demodulated signal from time domain waveform via a lock-in amplifier was analyzed. Figure 5c shows the measured output voltage in response to an applied 100 mHz H_{AC} varying from 0.1 to 10 nT. Clearly, a standard linear-response to H_{AC} within this range was obtained as given in the inset in Figure 5c. Accordingly, the limit of resolution (LOR) of the ME sensor based on this amplitude modulation method was determined to be as low as 100 pT. To confirm this LOR, Figure 5d further verified it by measurement. Considering an equivalent noise bandwidth (ENBW)of 7.8 Hz corresponding to the given measurement system, the calculated LoD was then calculated as 33 pT/√Hz at 0.1 Hz.

3.2. Resonant-Frequency Magnetic Sensor

ME laminates can be viewed as resonators from the perspective of mechanics and resonant phenomenon is also able to enhance the ME coupling coefficient and thus to improve the detection ability [10]. In this regard, ME sensors could be highly competitive over other magnetic field sensors, e.g., fluxgate sensor and optical pump magnetometer. Using a 2-2 ME composite, Dong et al. reported an enhanced LoR of 1.2 pT early in 2005 (see Figure 6a) [29]. As for MEMS ME magnetic sensor, Yarar et al. developed a low temperature deposition route of very high quality AlN film, allowing the reversal process flow. Correspondingly, the LoD was enhanced by almost an order of magnitude approaching 400 fT/$Hz^{1/2}$ at the electromechanical resonance, as shown in Figure 6b [43]. Based on the giant resonance ME coupling coefficient in 1-1 type ME laminate, a superhigh resonant magnetic-field sensitivity close to be 135 fT (see Figure 6c) was further obtained by Chu et al. [8], which indicates great potential for 1-1 type ME composites in the field of eddy current sensing, space magnetic sensing and active magnetic localizing [8][61]. In 2018 Turutin et al. reported a new ME composite consisting of the y + 140° cut congruent lithium niobate piezoelectric plates with an antiparallel polarized “head-to-head” bidomain structure and magnetostrictive material Metglas [44]. Based on this 2-2 ME bimorph, the equivalent magnetic noise spectral density was only 92 fT/$Hz^{1/2}$ and the directly measured resolution was found to be 200 fT at a bending resonance frequency of 6862 Hz (see Figure 6d), but one should note that the bandwidth of resonant ME sensors is normally below 1 kHz due to the high mechanical quality factor, which is a major limitation facing practical engineering applications [8][44][62]. It should however be noted that resonant ME sensors are greatly limited by the narrow bandwidth and specifically suited applications need to be considered.

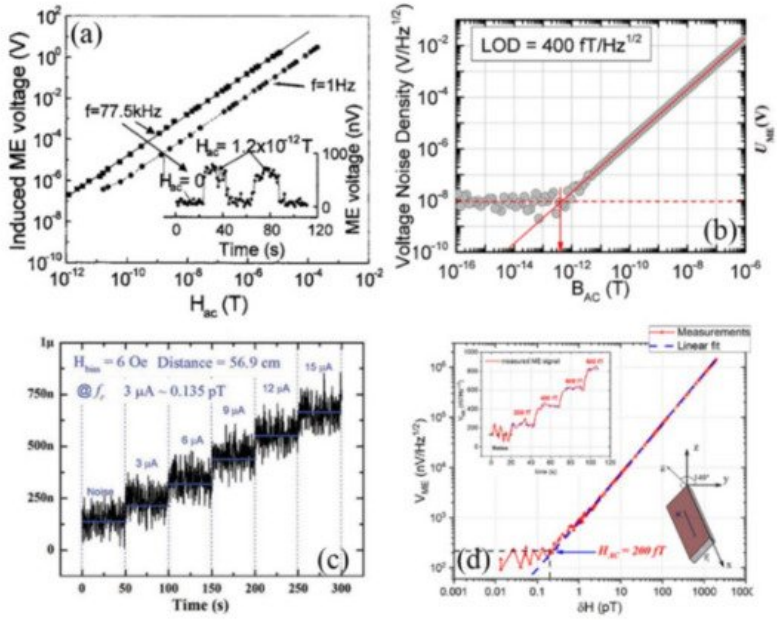

Figure 6. (**a**) Magnetic field detection limit measurements at frequencies of f = 1 Hz and f = 77.5 kHz (resonance condition), respectively [29]; (**b**)The measurement of LOD for MEMS ME sensor [43], (**c**) for 1-1 typed ME sensor [8] and (**d**) for a 2-2 ME bimorph [44].

3.3. DC Magnetic Sensor

DC or quasi-static magnetic sensors are promising for magnetic anomaly detection uses, such as geomagnetic navigation, metal detection and magnetic medical diagnosis, etc. Early in 2011, Gao et al. demonstrated the excellent detection ability for DC field using 2-1 ME composite [31]. As shown in Figure 7a,b, the magnetic resolution was found to be 4 nT and 1 nT when driving the composite at non-resonant frequency and resonance frequency, respectively [31]. In 2013, Nan et al. reported a self-biased 215 MHz magnetoelectric NEMS resonator consisting of an AlN/(FeGaB/Al_2O_3) multilayered heterostructure (Figure 7c), for ultra-sensitive DC magnetic field detection [51]. An ultra-sensitive detection level starting from 300 picoTesla was obtained experimentally (Figure 7d) [51]. The RF NEMS magnetoelectric sensor is compact, power efficient and readily integrated with CMOS technology, however, the measurement of the resonance frequency and the admittance spectrum is not technologically convenient. Li et al. then further proposed to monitor the reflected output voltage from the ME resonator directly [26]. The optimized detection sensitivity was determined as 2.8 Hz/nT for AlN/FeGaB resonator. An ultra-high frequency (UHF) lock-in amplifier and a directional coupler were used to apply and test the RF signal of this resonator. And the final limit of detection was measured to be around 0.8 nT.

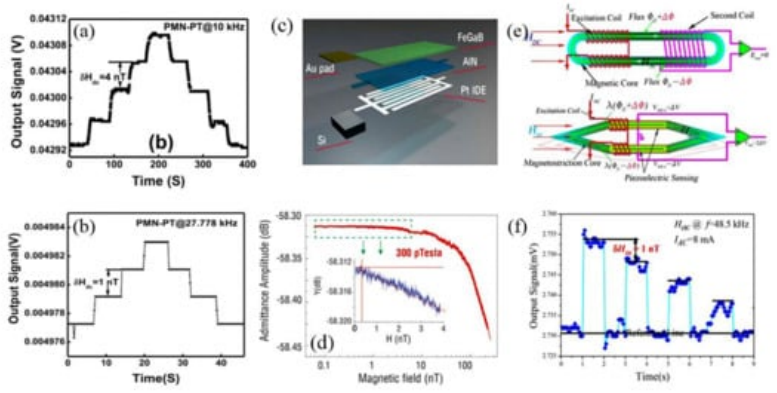

Figure 7. The measurement of LoD for Metglas/PMN–PT ME laminate at (**a**) *f* = 10 kHz and (**b**) resonance frequency of 27.778 kHz [31]. (**c**) Schematic representation and (**d**) the measurement of LoD for NMES AlN/(FeGaB/Al_2O_3) multilayered heterostructure [51]; (**e**) Schematic representation of the conventional flux gate senor and the proposed ME flux gate sensor [63]; (**f**) The measured results for DC magnetic field resolution [63].

Using the nonlinear resonance magnetoelectric effect in ME composites, Burdin et al. fabricated a planar langatate-Metglas structure and employed the third harmonics of the output signal to measure the DC magnetic field as low as 10 nT [64]. In addition, a broad dynamic range from ~10 nT to about 0.4 mT was also successfully obtained using the nonlinear ME effect [65]. More recently, Chu et al. proposed a shuttle-shaped, non-biased magnetoelectric flux gate sensor (MEFGS) for DC magnetic field sensing enlightened by the design of conventional flux gate sensor [63]. Figure 7e shows

both the schematic of typical flux gate senor and the proposed magnetoelectric flux gate sensor. The flux gate sensor based on Faraday's Law of Induction is composed of a racetrack type magnetic core surrounded by an excitation (first) coil and a detection (second) coil. With respect to MEFGS, a similar differential structure, which can produce a longitudinal-bending vibration when applying a DC field, can reject in-phase vibration noise and enhance the out-of-phase ME voltage signal simultaneously [54]. We note here that in [54] the authors found that a ME flux gate sensor excited under a non-resonant high frequency field could perform better detection ability. As shown in Figure 7f, the relative change of the ME voltage output signal in response to a LOD of 1 nT is around 0.2% and the output signal can return to the reference level during the repeated test cycles when choosing a non-resonant frequency of 48.5 kHz [63].

Performance summary of some typical magnetoelectric sensors was given in Table 2. Table 3 further compares the LoD of passive ME sensors with some commercially available magnetometers, i.e., magnetoresistive sensors, giant magneto-impedance sensors, fluxgate sensors, optically pumped magnetometers and SQUID magnetometers. As it can be seen in Table 3, ME sensor shows comparable and competitive performance with these products. Specifically, the low power consumption and high detection ability are significant advantages for ME sensors, while vibration interference still now greatly limits the engineering applications. On the other hand, piezoelectric materials are normally susceptible to the working temperature and the temperature stability of ME sensors is also a critical issue. For example, Burdin et al. compared the temperature dependence of the resonant magnetoelectric effect in several kinds of ME composites and showed that the widely studied PZT-Metglas ME sensor can only work in a narrow temperature range of 0 °C to +50 °C [66].

Table 2. Performance summary of typical magnetoelectric sensors.

	Composition	Working Mode	Sensing Mode	LoD
Low-frequency magnetic field sensing	Metglas/Mn-PMNT [67]	Longitudinal vibration (Multi-L-T)	Passive sensing	0.87 pT/√Hz @ 30 Hz
	Metglas/PMN-PT [33]	Longitudinal vibration (Multi-push-pull)	Passive sensing	5.1 pT/√Hz @ 1 Hz
	Metglas/PMN-PZT [55]	Longitudinal vibration (L-T)	Active Modulation	33 pT/√Hz @ 0.1 Hz
Resonant magnetic field sensing	Metglas/ LiNbO3 [44]	bending mode	Direct Sensing	92 fT/ √Hz
	FeCoSiB/(Pt)/AlN [43]	bending mode	Direct Sensing	400 fT/ √Hz
	Metglas/PMN-PZT [8]	Longitudinal vibration (L-T)	Direct Sensing	123 fT/ √Hz
DC magnetic field sensing	langatate-Metglas [64]	bending mode	Nonlinear ME effect	10 nT
	Metglas/PMN-PZT [9]	Longitudinal vibration (L-T)	Linear ME effect	1 nT
	FeCoSiB/(Pt)/AlN [26]	Lateral vibration	Delta-E effect	0.8 nT
	FeCoSiB/(Pt)/AlN [51]	Lateral vibration	Delta-E effect	0.4 nT

Table 3. Performance Comparison with commercially available magnetometer for 1 Hz magnetic field sensing.

Magnetometer	Working Temperature	Power Consumption (mW)	Typical Size	LoD@1Hz ($pT/\sqrt{Hz}$)	Limitations
ME sensor [33]	0 °C to +50 °C ①	<1	80 mm × 10 mm @ ME composites	5.1	Vibration interference
Magnetoresistive sensor ②	−40 °C to +125 °C	~0.02	6 mm × 5 mm × 1.5 mm @ sensing element	100	Low sensitivity
Giant magneto-impedance sensor ③	−20 °C to +60 °C	75	35 mm × 11 mm × 4.6 mm @ sensing element	15–25	Low sensitivity
Fluxgate magnetometer ④	−40 °C to +70 °C	350	ø100 mm × 125 mm @ system size	2–6	Power consumption
Optically pumped magnetometer ⑤	−35 °C to +50 °C	>12,000	175 cm × 28 cm × 28 cm @ system size	4	Complex setup
SQUID magnetometer [68]	<−196 °C	>1000	12.5 mm × 12.5 mm @ chip size	<0.005	Cooling

① Estimated from the data in ref. [64]; ② Based on commercial product TMR9001 in MultiDimension Technology Co., Ltd. (Zhangjiagang Free Trade Zone, Jiangsu Province, China); ③ Based on commercial product MI-CB-1DH in AICHI STEEL CORPORATION (Tōkai city, Aichi Prefecture, Japan); ④ Based on commercial product Mag03 from Bartington Instruments Ltd (Witney, Oxon, OX28 4GG United Kingdom).; ⑤ Based on commercial product G882 marine magnetometer from GEOMETRICS, INC (San Jose, CA, USA).

4. Engineering Applications of ME Sensors

As we summarized in Table 2 and Table 3, ME sensors show competitive performance with commercial optically pumped magnetometers, giant magneto-impedance sensors and fluxgate magnetometers. In this regard, a large number of works that utilize ME sensors for magnetic field sensing have been published and various applications have been implemented.

References

1. Ma, J.; Hu, J.; Li, Z.; Nan, C.W. Recent progress in multiferroic magnetoelectric composites: From bulk to thin films. Adv. Mater. 2011, 23, 1062–1087.
2. Hu, J.-M.; Nan, T.; Sun, N.X.; Chen, L.-Q. Multiferroic magnetoelectric nanostructures for novel device applications. MRS Bull. 2015, 40, 728–735.
3. Hu, J.-M.; Duan, C.-G.; Nan, C.-W.; Chen, L.-Q. Understanding and designing magnetoelectric heterostructures guided by computation: Progresses, remaining questions, and perspectives. NPJ Comput. Mater. 2017, 3, 1–21.

4. Kleemann, W. Multiferroic and magnetoelectric nanocomposites for data processing. J. Phys. D Appl. Phys. 2017, 50, 223001.
5. Lawes, G.; Srinivasan, G. Introduction to magnetoelectric coupling and multiferroic films. J. Phys. D Appl. Phys. 2011, 44, 243001.
6. Palneedi, H.; Annapureddy, V.; Priya, S.; Ryu, J. Status and Perspectives of Multiferroic Magnetoelectric Composite Materials and Applications. Actuators 2016, 5, 9.
7. Chu, Z.; PourhosseiniAsl, M.; Dong, S. Review of multi-layered magnetoelectric composite materials and devices applications. J. Phys. D Appl. Phys. 2018, 51, 243001.
8. Chu, Z.; Shi, H.; Shi, W.; Liu, G.; Wu, J.; Yalng, J.; Dong, S. Enhanced Resonance Magnetoelectric Coupling in (1-1) Connectivity Composites. Adv. Mater. 2017, 29, 1606022.
9. PourhosseiniAsl, M.; Gao, X.; Kamalisiahroudi, S.; Yu, Z.; Chu, Z.; Yang, J.; Lee, H.-Y.; Dong, S. Versatile power and energy conversion of magnetoelectric composite materials with high efficiency via electromechanical resonance. Nano Energy 2020, 70, 104506.
10. Nan, C.-W.; Bichurin, M.I.; Dong, S.; Viehland, D.; Srinivasan, G. Multiferroic magnetoelectric composites: Historical perspective, status, and future directions. J. Appl. Phys. 2008, 103, 031101.
11. Fiebig, M. Revival of the magnetoelectric effect. J. Phys. D Appl. Phys. 2005, 38, R123–R152.
12. Zhai, J.; Xing, Z.; Dong, S.; Li, J.; Viehland, D. Magnetoelectric Laminate Composites: An Overview. J. Am. Ceram. Soc. 2008, 91, 351–358.
13. Wang, Y.; Li, J.; Viehland, D. Magnetoelectrics for magnetic sensor applications: Status, challenges and perspectives. Mater. Today 2014, 17, 269–275.
14. Gutierrez, J.; Lasheras, A.; Martins, P.; Pereira, N.; Barandiaran, J.M.; Lanceros-Mendez, S. Metallic Glass/PVDF Magnetoelectric Laminates for Resonant Sensors and Actuators: A Review. Sensors 2017, 17, 1251.
15. Sreenivasulu, G.; Qu, P.; Petrov, V.; Qu, H.; Srinivasan, G. Sensitivity Enhancement in Magnetic Sensors Based on Ferroelectric-Bimorphs and Multiferroic Composites. Sensors 2016, 16, 262.
16. Annapureddy, V.; Palneedi, H.; Hwang, G.-T.; Peddigari, M.; Jeong, D.-Y.; Yoon, W.-H.; Kim, K.-H. Magnetic energy harvesting with magnetoelectrics: An emerging technology for self-powered autonomous systems. Sustain. Energy Fuels 2017, 1, 2039–2052.
17. Vopson, M.M. Fundamentals of Multiferroic Materials and Their Possible Applications. Crit. Rev. Solid State Mater. Sci. 2015, 40, 223–250.
18. Gao, X.; Yan, Y.; Carazo, A.V.; Dong, S.; Priya, S. Low-temperature cofired unipoled multilayer piezoelectric transformers. IEEE Trans. Ultrason. Ferroelectr. Freq. Control 2017, 65, 513–519.
19. Yang, N.; Wu, H.; Wang, S.; Yuan, G.; Zhang, J.; Sokolov, O.; Bichurin, M.I.; Wang, K.; Wang, Y. Ultrasensitive flexible magnetoelectric sensor. APL Mater. 2021, 9, 021123.
20. Dong, S.; Liu, J.-M.; Cheong, S.-W.; Ren, Z. Multiferroic materials and magnetoelectric physics: Symmetry, entanglement, excitation, and topology. Adv. Phys. 2015, 64, 519–626.
21. Astrov, D.N. Magnetoelectric Effect In Chromium Oxide. Sov. Phys. Jetp 1961, 13, 729–733.
22. Schmid, H. Multi-ferroic magnetoelectrics. Ferroelectrics 1994, 162, 317–338.
23. Catalan, G.; Scott, J.F. Physics and Applications of Bismuth Ferrite. Adv. Mater. 2009, 21, 463–2485.
24. Yamauchi, K.; Picozzi, S. Orbital degrees of freedom as origin of magnetoelectric coupling in magnetite. Phys. Rev. B 2012, 85, 085131.
25. Pantinakis, A.; Jackson, D.A. High-sensitivity low-frequency magnetometer using magnetostrictive primary sensing and piezoelectric signal recovery. Electron. Lett. 1986, 22, 737–738.
26. Li, M.; Matyushov, A.; Dong, C.; Chen, H.; Lin, H.; Nan, T.; Qian, Z.; Rinaldi, M.; Lin, Y.; Sun, N.X. Ultra-sensitive NEMS magnetoelectric sensor for picotesla DC magnetic field detection. Appl. Phys. Lett. 2017, 110, 143510.
27. Ryu, J.; Priya, S.; Uchino, K.; Kim, H.-E. Magnetoelectric Effect in Composites of Magnetostrictive and Piezoelectric Materials. J. Electroceramics 2002, 8, 107–119.
28. Dong, S.; Li, J.-F.; Viehland, D. Ultrahigh magnetic field sensitivity in laminates of TERFENOL-D and Pb(Mg1/3Nb2/3)O3–PbTiO3 crystals. Appl. Phys. Lett. 2003, 83, 2265–2267.
29. Dong, S.; Zhai, J.; Bai, F.; Li, J.-F.; Viehland, D. Push-pull mode magnetostrictive/piezoelectric laminate composite with an enhanced magnetoelectric voltage coefficient. Appl. Phys. Lett. 2005, 87, 062502.

30. Dong, S.; Zhai, J.; Li, J.; Viehland, D. Near-ideal magnetoelectricity in high-permeability magnetostrictive/piezofiber laminates with a (2-1) connectivity. Appl. Phys. Lett. 2006, 89, 252904.

31. Gao, J.; Shen, L.; Wang, Y.; Gray, D.; Li, J.; Viehland, D. Enhanced sensitivity to direct current magnetic field changes in Metglas/Pb(Mg1/3Nb2/3)O3–PbTiO3 laminates. J. Appl. Phys. 2011, 109, 074507.

32. Li, M.; Gao, J.; Wang, Y.; Gray, D.; Li, J.; Viehland, D. Enhancement in magnetic field sensitivity and reduction in equivalent magnetic noise by magnetoelectric laminate stacks. J. Appl. Phys. 2012, 111, 104504.

33. Wang, Y.; Gray, D.; Betrry, D.; Gao, J.; Li, M.; Li, J.; Viehland, D. An extremely low equivalent magnetic noise magnetoelectric sensor. Adv. Mater. 2011, 23, 4111–4114.

34. Li, M.; Berry, D.; Das, J.; Gray, D.; Li, J.; Viehland, D. Enhanced Sensitivity and Reduced Noise Floor in Magnetoelectric Laminate Sensors by an Improved Lamination Process. J. Am. Ceram. Soc. 2011, 94, 3738–3741.

35. Gao, J.; Das, J.; Xing, Z.; Li, J.; Viehland, D. Comparison of noise floor and sensitivity for different magnetoelectric laminates. J. Appl. Phys. 2010, 108, 084509.

36. Ma, J.; Shi, Z.; Nan, C.W. Magnetoelectric Properties of Composites of Single Pb(Zr,Ti)O3 Rods and Terfenol-D/Epoxy with a Single-Period of 1-3-Type Structure. Adv. Mater. 2007, 19, 2571–2573.

37. Shi, Z.; Nan, C.W.; Zhang, J.; Cai, N.; Li, J.-F. Magnetoelectric effect of Pb(Zr,Ti)O3 rod arrays in a (Tb,Dy)Fe2/epoxy medium. Appl. Phys. Lett. 2005, 87, 012503.

38. Srinivasan, G.; Rasmussen, E.T.; Gallegos, J.; Srinivasan, R.; Bokhan, Y.I.; Laletin, V.M. Magnetoelectric bilayer and multilayer structures of magnetostrictive and piezoelectric oxides. Phys. Rev. B 2001, 64, 214408.

39. Zhai, J.; Dong, S.; Xing, Z.; Li, J.; Viehland, D. Giant magnetoelectric effect in Metglas/polyvinylidene-fluoride laminates. Appl. Phys. Lett. 2006, 89, 083507.

40. Jin, J.; Lu, S.-G.; Chanthad, C.; Zhang, Q.; Haque, M.A.; Wang, Q. Multiferroic Polymer Composites with Greatly Enhanced Magnetoelectric Effect under a Low Magnetic Bias. Adv. Mater. 2011, 23, 3853.

41. Sreenivasulu, G.; Fetisov, L.Y.; Fetisov, Y.K.; Srinivasan, G. Piezoelectric single crystal langatate and ferromagnetic composites: Studies on low-frequency and resonance magnetoelectric effects. Appl. Phys. Lett. 2012, 100, 052901.

42. Kirchhof, C.; Krantz, M.; Teliban, I.; Jahns, R.; Marauska, S.; Wagner, B.; Knoöchel, R.; Gerken, M.; Meyners, D.; Quandt, E. Giant magnetoelectric effect in vacuum. Appl. Phys. Lett. 2013, 102, 232905.

43. Yarar, E.; Salzer, S.; Hrkac, V.; Piorra, A.; Höft, M.; Knöchel, R.; Kienle, L.; Quandt, E. Inverse bilayer magnetoelectric thin film sensor. Appl. Phys. Lett. 2016, 109, 022901.

44. Turutin, A.V.; Vidal, J.V.; Kubasov, I.V.; Kislyuk, A.M.; Malinkovich, M.D.; Parkhomenko, Y.N.; Kobeleva, S.P.; Pakhomov, O.V.; Kholkin, A.L.; Sobolev, N.A. Magnetoelectric metglas/bidomain y + 140°-cut lithium niobate composite for sensing fT magnetic fields. Appl. Phys. Lett. 2018, 112, 262906.

45. Palneedi, H.; Choi, S.-Y.; Kim, G.; Annapureddy, V.; Maurya, D.; Priya, S.; Lee, K.J.; Chung, S.; Kang, S.L.; Ryu, J. Tailoring the Magnetoelectric Properties of Pb(Zr,Ti)O3 Film Deposited on Amorphous Metglas Foil by Laser Annealing. J. Am. Ceram. Soc. 2016, 99, 2680–2687.

46. Palneedi, H.; Maurya, D.; Kim, G.-Y.; Priya, S.; Kang, S.-J.L.; Kim, K.-H.; Choi, S.-Y.; Ryu, J. Enhanced off-resonance magnetoelectric response in laser annealed PZT thick film grown on magnetostrictive amorphous metal substrate. Appl. Phys. Lett. 2015, 107, 012904.

47. Palneedi, H.; Yeo, H.G.; Hwang, G.-T.; Annapureddy, V.; Kim, J.-W.; Choi, J.-J.; Trolier-McKinstry, S.; Ryu, J. A flexible, high-performance magnetoelectric heterostructure of (001) oriented Pb(Zr0.52Ti0.48)O3 film grown on Ni foil. Appl. Mater. 2017, 5, 096111.

48. Palneedi, H.; Maurya, D.; Kim, G.-Y.; Annapureddy, V.; Noh, M.-S.; Kang, C.-Y.; Kim, J.-W.; Choi, J.-J.; Choi, S.-Y.; Chung, S.-Y.; et al. Unleashing the Full Potential of Magnetoelectric Coupling in Film Heterostructures. Adv. Mater. 2017, 29, 1605688.

49. Greve, H.; Woltermann, E.; Quenzer, H.-J.; Wagner, B.; Quandt, E. Giant magnetoelectric coefficients in (Fe90Co10)78Si12B10-AlN thin film composites. Appl. Phys. Lett. 2010, 96, 182501.

50. Jovičević Klug, M.; Thormählen, L.; Röbisch, V.; Toxværd, S.D.; Höft, M.; Knöchel, R.; Quandt, E.; Meyners, D.; McCord, J. Antiparallel exchange biased multilayers for low magnetic noise magnetic field sensors. Appl. Phys. Lett. 2019, 114, 192410.

51. Nan, T.; Hui, Y.; Rinaldi, M.; Sun, N.X. Self-biased 215 MHz magnetoelectric NEMS resonator for ultra-sensitive DC magnetic field detection. Sci. Rep. 2013, 3, 1985.

52. Tu, C.; Chu, Z.-Q.; Spetzler, B.; Hayes, P.; Dong, C.-Z.; Liang, X.-F.; Chen, H.-H.; He, Y.-F.; Wei, Y.-Y.; Lisenkov, I.; et al. Mechanical-Resonance-Enhanced Thin-Film Magnetoelectric Heterostructures for Magnetometers, Mechanical

Antennas, Tunable RF Inductors, and Filters. Materials 2019, 12, 2259.

53. Nan, T.; Lin, H.; Gao, Y.; Matyushov, A.; Yu, G.; Chen, H.; Sun, N.; Wei, S.; Wang, Z.; Li, M.; et al. Acoustically actuated ultra-compact NEMS magnetoelectric antennas. Nat. Commun 2017, 8, 296.
54. Chu, Z.; Shi, H.; Gao, X.; Wu, J.; Dong, S. Magnetoelectric coupling of a magnetoelectric flux gate sensor in vibration noise circumstance. AIP Adv. 2018, 8, 015203.
55. Fang, C.; Jiao, J.; Ma, J.; Lin, D.; Xu, H.; Zhao, X.; Luo, H. Significant reduction of equivalent magnetic noise by in-plane series connection in magnetoelectric Metglas/Mn-doped Pb(Mg1/3Nb2/3)O3-PbTiO3laminate composites. J. Phys. D Appl. Phys. 2015, 48, 465002.
56. Liu, Y.; Jiao, J.; Ma, J.; Ren, B.; Li, L.; Zhao, X.; Luo, H.; Shi, L. Frequency conversion in magnetoelectric composites for quasi-static magnetic field detection. Appl. Phys. Lett. 2013, 103, 212902.
57. Petrie, J.R.; Fine, J.; Mandal, S.; Sreenivasulu, G.; Srinivasan, G.; Edelstein, A.S. Enhanced sensitivity of magnetoelectric sensors by tuning the resonant frequency. Appl. Phys. Lett. 2011, 99, 043504.
58. Petrie, J.; Mandal, S.; Gollapudi, S.; Viehland, D.; Gray, D.; Srinivasan, G.; Edelstein, A.S. Enhancing the sensitivity of magnetoelectric sensors by increasing the operating frequency. J. Appl. Phys. 2011, 110, 124506.
59. Ou-Yang, J.; Liu, X.; Zhou, H.; Zou, Z.; Yang, Y.; Li, J.; Zhang, Y.; Zhu, B.; Chetn, S.; Yang, X. Magnetoelectric laminate composites: An overview of methods for improving the DC and low-frequency response. J. Phys. D Appl. Phys. 2018, 51, 324005.
60. Chu, Z.; Dong, C.; Tu, C.; Liang, X.; Chen, H.; Sun, C.; Yu, Z.; Dong, S.; Sun, N.-X. A low-power and high-sensitivity magnetic field sensor based on converse magnetoelectric effect. Appl. Phys. Lett. 2019, 115, 162901.
61. Chu, Z.; Yu, Z.; PourhosseiniAsl, M.; Tu, C.; Dong, S. Enhanced low-frequency magnetic field sensitivity in magnetoelectric composite with amplitude modulation method. Appl. Phys. Lett. 2019, 114, 132901.
62. PourhosseiniAsl, M.; Yu, Z.; Chu, Z.; Yang, J.; Xu, J.; Hou, Y.; Dong, S. Enhanced self-bias magnetoelectric effect in locally heat-treated ME laminated composite. Appl. Phys. Lett. 2019, 115, 112901.
63. Li, J.; Ma, G.; Zhang, S.; Wang, C.; Jin, Z.; Zong, W.; Zhao, G.; Wang, X.; Xu, J.; Cao, D.; et al. AC/DC dual-mode magnetoelectric sensor with high magnetic field resolution and broad operating bandwidth. AIP Adv. 2021, 11, 045015.
64. Chu, Z.; Shi, H.; PourhosseiniAsl, M.J.; Wu, J.; Shi, W.; Galo, X.; Yuan, X.; Dong, S. A magnetoelectric flux gate: New approach for weak DC magnetic field detection. Sci. Rep. 2017, 7, 8592.
65. Burdin, D.A.; Chashin, D.V.; Ekonomov, N.A.; Fetisov, Y.K.; Stashkevich, A.A. High-sensitivity dc field magnetometer using nonlinear resonance magnetoelectric effect. J. Magn. Magn. Mater. 2016, 405, 244–248.
66. Burdin, D.; Chashin, D.; Ekonomov, N.; Fetisov, L.; Fetisov, Y.; Shamonin, M. DC magnetic field sensing based on the nonlinear magnetoelectric effect in magnetic heterostructures. J. Phys. D Appl. Phys. 2016, 49, 375002.
67. Burdin, D.A.; Ekonomov, N.A.; Chashin, D.V.; Fetisov, L.Y.; Fetisov, Y.K.; Shamonin, M. Temperature Dependence of the Resonant Magnetoelectric Effect in Layered Heterostructures. Materials 2017, 10, 1183.
68. Schmelz, M.; Stolz, R.; Zakosarenko, V.; Schönau, T.; Anders, S.; Fritzsch, L.; Mück, M.; Meyer, M.; Meyer, H.-G. Sub-fT/Hz1/2 resolution and field-stable SQUID magnetometer based on low parasitic capacitance sub-micrometer cross-type Josephson tunnel junctions. Phys. C Supercond. Its Appl. 2012, 482, 27–32.

Retrieved from https://encyclopedia.pub/entry/history/show/25008